PERGAMON

Journal of Structural Geology 24 (2002) 1633–1646

JOURNAL OF STRUCTURAL GEOLOGY

www.elsevier.com/locate/jstrugeo

Crystallographic orientation, chemical composition and three-dimensional geometry of sigmoidal garnet: evidence for rotation

Takeshi Ikeda[a,*], Norimasa Shimobayashi[b], Simon R. Wallis[b,1], Akira Tsuchiyama[c]

[a]*Department of Earth and Planetary Sciences, Graduate School of Science, Kyushu University, 33 Hakozaki, Fukuoka, 812-8581 Japan*
[b]*Department of Geology and Mineralogy, Graduate School of Science, Kyoto University, Kyoto, 606-8502 Japan*
[c]*Department of Earth and Space Science, Graduate School of Science, Osaka University, Toyonaka, Osaka, 560-0043 Japan*

Received 15 March 2001; revised 7 November 2001; accepted 14 November 2001

Abstract

Studies of the microstructure, crystallographic orientation, chemical composition and three-dimensional shape of sigmoidal garnet reveal a number of features that can be used to discuss its origin, and in particular to distinguish between rotational versus non-rotational models. Crystallographic orientation mapping of sigmoidal garnet shows no evidence of subgrain formation or of being polycrystalline, suggesting that neither ductile nor brittle deformation is significant. Chemical mapping shows that the garnet grew during a single metamorphic event, arguing against ideas that sigmoidal garnet forms as the result of a series of independent growth events. The chemical mapping also reveals anisotropic growth of garnet with the long axis of the ellipsoidal grain rotating in the same direction but to a lesser degree than the inclusion trails. This is best explained as the result of syn-growth rotation of the garnet with respect to the foliation and maximum growth direction. High-resolution X-ray CT scanning shows that the inclusion trails have a complex three-dimensional spiral geometry. This type of geometry is predicted by rotational models of sigmoidal garnet formation.

Keywords: Crystallographic orientation; Chemical composition; Three-dimensional spiral geometry; Sigmoidal garnet; Rotation

1. Introduction

Garnets with curved inclusion trails are commonly referred to as 'snowball' or 'sigmoidal' garnets and are a common feature of regional metamorphic rocks. The inclusion trails are commonly very similar in composition and show good continuation with the external foliation, suggesting that they represent foliation that has been incorporated within the garnet during its growth. There is, however, considerable debate on how to account for the curvature of the inclusion trails. One school of thought, the 'rotationalists', considers that these microstructures form in a single phase of garnet growth and the curvature is due to syn-growth rotation of the garnet with respect to the foliation (e.g. Zwart, 1962; Rosenfeld, 1970; Schoneveld, 1977). In this interpretation the two-fold symmetry axis of the inclusion trails lies parallel to the rotation axis of finite deformation and can be used as a sense of shear indicator. A second school, the 'non-rotationalists', proposes that garnet (and other porphyroblasts) maintain a fixed orientation with respect to the earth's horizontal (e.g. Bell and Johnson, 1989; Johnson, 1990; Bell et al., 1992; Hayward, 1992; Aerden, 1995; Hickey and Bell, 1999). In this second case, the tight curvature seen in many sigmoidal garnets is explained as the result of the garnet overgrowing a series of differently oriented foliations, and the symmetry axes of the inclusion trails are interpreted as the intersection of a series of independent foliations and are referred to as foliation intersection axes or FIAs (e.g. Bell et al., 1997, 1998; Bell and Mares, 1999). The consistent orientation of FIAs reported by a number of workers is considered to be one of the most crucial lines of evidence in support of non-rotation (e.g. Bell et al., 1995). The implications of the non-rotational model for sense of shear determinations, folding mechanisms, and orogenic processes are discussed by Bell et al. (1992, 1995) and Bell and Hickey (1997).

Most attempts to test the rotational and non-rotational models have focused on looking for microstructural evidence for or against rotation (Passchier et al., 1992; Visser and Mancktelow, 1992; Wallis, 1992). For a single grain, the question of whether the foliation or the garnet rotates is a semantic one and depends only on the reference frame chosen. For single grains, a more significant

* Corresponding author.
E-mail address: ikeda@geo.kyushu-u.ac.jp (T. Ikeda).
[1] Now at: Department of Earth and Planetary Sciences, Graduate School of Environmental Studies, Nagoya University, Nagoya 464-8602 Japan.

0191-8141/02/$ - see front matter
PII: S0191-8141(01)00160-2

difference is that the rotational model implies that sigmoidal garnet forms during a single phase of metamorphism and associated non-coaxial deformation, while the non-rotational model implies that the garnet preserves a polyphase history.

In this contribution we re-examine the problem of how sigmoidal garnet forms by combining three different types of studies. First, we used an X-ray microscope to study whether or not the garnet is a single crystal. The shear modulus and the creep strength of garnet are significantly higher than those of other silicates (Karato, 1989; Bass, 1995). This suggests that garnet is unlikely to undergo significant deformation under normal crustal conditions. However, deformation may affect garnet shape, as suggested by the following evidence. Tensile fractures were recognised in oblate garnet grains occurring in ductilely deformed rocks (e.g. Ji and Martignole, 1994). Laue X-ray diffraction photographs detected plastic deformation of garnet grains from mylonites formed at high temperatures (Dalziel and Bailey, 1968; Ji et al., 1997). In addition, in some cases the complex shapes of garnet are difficult to explain in terms of a single stage of nucleation and overgrowth and may be the result of impingement and welding of separate grains (e.g. Kamineni, 1978; Ikeda, 1993). The assumptions accepted by both the rotational and non-rotational schools that sigmoidal garnets were rigid single grains throughout their growth are open to question and their validity should be verified. In order to determine whether the sigmoidal garnet grains are polycrystalline or not, it is necessary to study variations in the crystallographic orientation of an individual sigmoidal garnet. To study this feature we used a newly-designed X-ray analytical microscope.

Second, we examined the relationship between chemical zoning patterns in sigmoidal garnet and the microstructure. Extensive petrographic and theoretical studies of chemical zoning of garnet have been very successful in revealing the associated growth and resorption histories (see Spear (1993) for a review). The original growth zoning can be used to determine the overall external shape of garnets during its growth (e.g. Spiess and Bell, 1996; Spear and Daniel, 2001). An important aspect of the non-rotational model is that the garnet should undergo a series of roughly orthogonal shape changes (e.g. Fig. 6 in Bell et al. (1992)). In contrast, rotational models predict either equidimensional growth or continuous change in orientation of the long axis. Chemical zoning patterns perhaps represent one of the best ways to test the non-rotational models. To our knowledge, however, this aspect of sigmoidal garnets has not before been explicitly studied. Qualitative X-ray mapping and quantitative chemical analyses were used to determine a chemical contour map of the sigmoidal grain. These studies reveal changes during growth both in the external shape of garnet and orientation of its long axis.

Third, we observed the three-dimensional (3-D) shape of the inclusion trails using X-ray computed tomography (CT). Rotational and non-rotational models make different predictions about the 3-D shape of the inclusion trails in sigmoidal garnet. This can potentially be used to distinguish the models. However, the true 3-D distribution of inclusions is difficult to observe. One approach is to study serial sections combined with observations using a universal stage microscope (e.g. Powell and Treagus, 1967, 1970; Johnson, 1993; Bell et al., 1995). However, important information can be lost during the sectioning and re-examination of the same samples is not possible. Sectioning at intervals of several millimetres is likely to be too large to judge whether inclusion trails trace continuously or discontinuously. In contrast, modern X-ray CT methods are non-destructive and it has been shown that this can be applied to rocks to determine 3-D structures such as location of crystals, crystal size and whether or not the crystals form clusters (e.g. Denison et al., 1997). Here we present a developed method for studying the 3-D shape of the internal fabrics of porphyroblasts using CT scanning with an unprecedentedly high resolution.

2. Analytical work

In this study, two metapelite samples both containing sigmoidal garnets were invesitgated, #80904 from the Dalradian rocks of NW Scotland and #MS95 from the Austroalpine nappes of the Eastern Alps. The analytical procedures are as below.

A specially-designed X-ray analytical microscope at Kyoto University was used to examine the crystallographic orientations of sigmoidal garnet grains to determine whether the sigmoidal garnet is a single crystal or polycrystalline. The X-ray microscope was constructed by combining a special goniometric stage with a conventional X-ray analytical microscope [HORIBA XGT-2000] (Shimobayashi et al., 1999). The goniometric stage is composed of a large tilting stage (χ-stage) and a rotation stage (ϕ-stage). A small X–Y scanning stage (± 10 mm in each direction) is mounted on the ϕ-stage. These stages can be controlled to a high level of accuracy with stepping motors controlled by two personal computers; one for the χ- and ϕ-stages and the other for the X–Y stage. An X-ray beam generated by a microfocus X-ray tube (Rh target) is focused onto a spot less than 10 μm in diameter with the working distance of 1 mm through the X-ray guide tube (XGT), and this irradiates the sample placed on the X–Y scanning stage. An energy-dispersive spectrometer (EDS) detects the fluorescent and back-scattered X-rays emitted from the sample. In the case of crystalline materials, the diffracted X-rays can also be detected with the EDS. By adjusting the χ- and ϕ-stages, we can obtain a strong and clear signal of the diffracted X-rays. If the sample is scanned by moving the X–Y stage with the χ- and ϕ-stages fixed, we can simultaneously obtain images of both the fluoresced and diffracted X-rays of a given area. The mapping of the

sigmoidal garnet was carried out under the conditions of 50 kV accelerating voltage, 1 mA tube current, 5×5 μm pixel size and 1000 ms dwelling time.

In order to examine chemical zoning of the garnet grain, we first employed a wavelength-dispersive X-ray analytical system (JEOL JXA-8800) with X-ray mapping software at Shiga University. A beam current of 20 nA and an accelerating voltage of 15 kV were used with a 2×2 μm pixel size for a 25 ms dwelling time. In total 1000×1000 pixels were obtained for the mapping. The chemical compositions of constituent minerals were determined using a scanning electron microscope (JEOL JSM-5800LV) combined with a Link ISIS analytical system at Kyushu University, under analytical conditions of 500 pA beam current, 20 kV accelerating voltage and 100 s livetime.

Three-dimensional structures of sigmoidal grains of garnet in sample #80904 were obtained by the X-ray CT. A rock specimen was imaged by a microfocus X-ray CT scanner, ELESCAN NX-NCP-C80-I(4) (Nittetsu Elex Co.) at Osaka University. The CT scanner has a microfocus X-ray tube (6×8 μm) with a W target and a CCD camera (54×72 mm and 480×640 pixels) as the X-ray detector. Details of this scanner are described in Tsuchiyama et al. (2002). A columnar sample was prepared from the rock to reduce imaging artifacts by the CT method. A large sample (15 mm in diameter and 15 mm in height) was imaged first to search garnet grains suitable for detailed imaging by using a smaller sample with higher resolution. CT slices perpendicular to the axis of the columnar sample were imaged at an X-ray accelerating voltage of 80 kV and tube current of 25 μA. The 3-D structure was obtained from 182 successive slices. Each CT image has 512×512 pixels with a magnification of four and the corresponding pixel size and slice width are 35.2×35.2 μm^2 and 84.4 μm, respectively.

A small columnar sample (4.5 mm in diameter and 4 mm in height), which contains full garnet grains, was removed from the large sample. This sample was imaged at 60 kV and 49 μA with higher magnification. The pixel size and the slice width became 10.5×10.5 μm^2 and 8.44 μm, respectively. This gives the spatial resolution of about 25 μm. For obtaining a cross-sectional image, 450 projections were obtained at 0.4° intervals during the rotation of the sample. The contrast of the projections was 14 bit resolution. To save the time needed for imaging, 13 slices were imaged at a time with a cone beam and this imaging process was repeated 22 times by successively changing the sample height position. Although a cone beam correction was not made, the shapes of garnet grains in the CT images were not greatly affected by the cone beam because the number of the images taken at one time was small. The 3-D structure was obtained from 360 slices. The total time taken for the detailed images was about 2 h for taking the X-ray projections and about 3 h for reconstruction of CT images from the projections. A single crystal of olivine from San Carlos, USA, which was used as a standard for identifying mineral phases in the rock sample, was embedded in a columnar container (4.5 mm in diameter) of silicon powder with a resin according to Tsuchiyama et al. (2002). This was also imaged under the same conditions as the sample.

3. Sample descriptions

3.1. Geological setting

The first sample, #80904, is from the NW part of the Dalradian rocks in the Loch Leven area, Inverness-shire, Scotland. Two stages of deformation (D_1, D_2) are responsible for the major structures of the area (Bailey and Maufe, 1960; Treagus, 1974; Ikeda, 1996). The first phase of deformation is responsible for tight folding of the original stratigraphic sequence, which is associated with the formation of an axial planar schistosity. This foliation (S_1) is sub-parallel to the bedding plane throughout the area except for local exposures of closures of tight D_1 folds. The second phase of deformation (D_2) includes deflection of both stratigraphy and the D_1 fold axial surface. D_2 deformation is associated with the formation of a crenulation cleavage (S_2). The second foliation (S_2) is deflected around garnet grains that include the strongly curved S_1 fabric (Treagus, 1974). No clear stretching lineation is observed. This may be either because it was not developed originally or, alternatively, because it has been obliterated by the effect of subsequent deformation and recrystallisation. Locally, cross-bedding is well preserved in quartzite layers (Bailey and Maufe, 1960) suggesting relatively low strain. The well-developed foliation in the metapelite lithologies implies, however, that this rock type has undergone considerably higher strain.

The area belongs to the garnet zone as defined by Bailey (1923). The metamorphic conditions of the garnet zone of the Dalradian rocks are estimated to be around 6 kbar and 500 °C (Richardson and Powell, 1976; Pattison, 1989; Pattison and Voll, 1991). Pattison and Voll (1991) have proposed the following reaction that accounts for the formation of garnet:

$$\text{muscovite} + \text{chlorite} + \text{quartz} = \text{garnet} + \text{biotite} + H_2O - \text{fluid}. \quad (1)$$

The second sample, #MS95, is a metapelite from within a broad kilometre-scale shear zone along the base of the Austroalpine nappes of the Eastern Alps (for detailed description see Wallis and Behrmann (1996)). Within this shear zone there are penetrative ductile fabrics related to both crustal thickening associated with prograde metamorphism (D_r) and crustal thinning associated with retrograde metamorphism (D_s). In both deformation phases the stretching direction is oriented W to NW and the tectonic fabrics show a general monoclinic symmetry suggesting non-coaxial deformation with the vorticity vector parallel

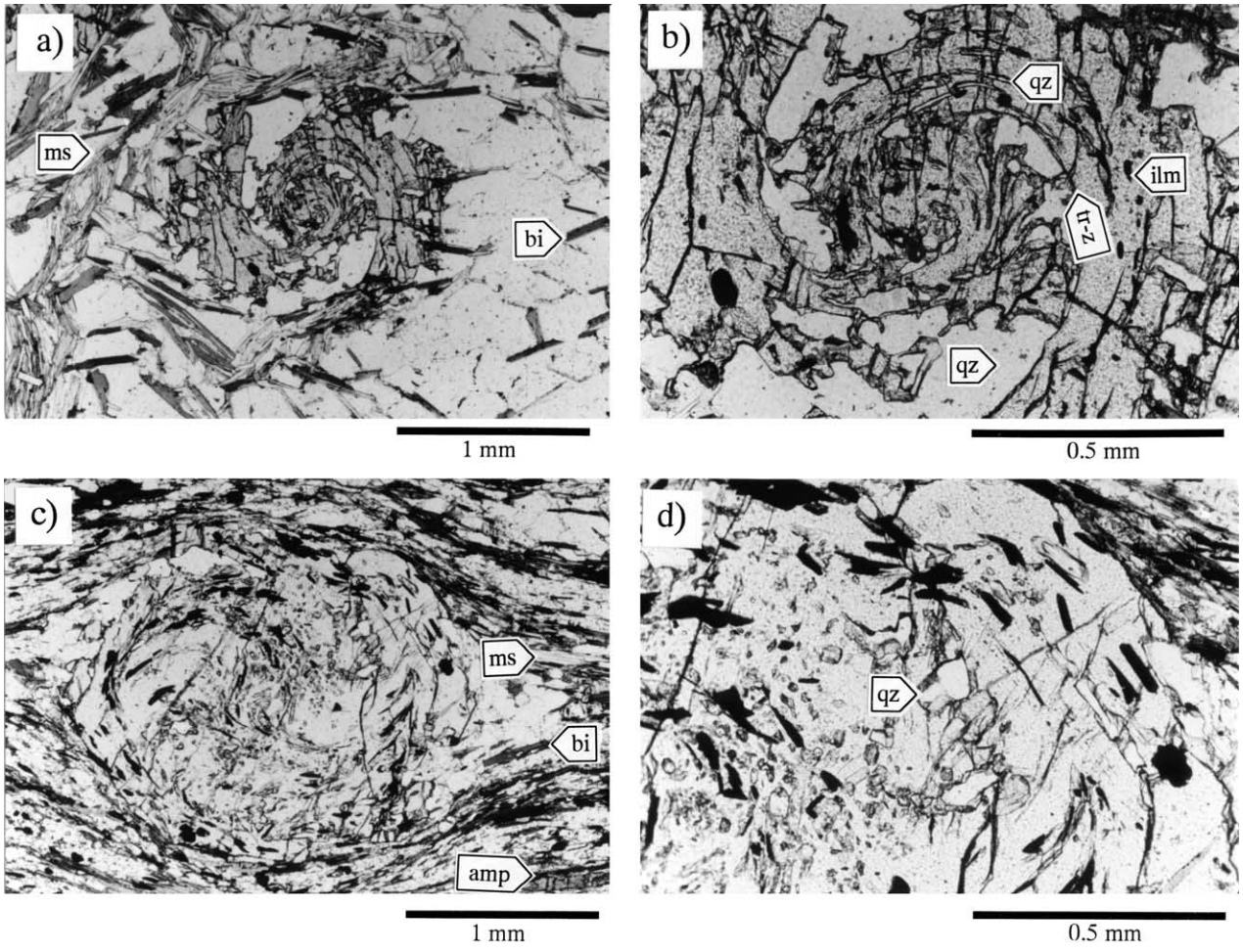

Fig. 1. Photomicrographs of sigmoidal garnet. (a) Sample #80904 from the Dalradian metamorphic region. (b) Detail of (a). (c) Sample #MS95 from the western Alps. (d) Detail of (c). All photomicrographs in plane polarised light. Abbreviations: tr-z, truncation zone; ms, muscovite; bi, biotite; ilm, ilmenite; qz, quartz; amp, amphibole.

to the intermediate principal axis of finite strain and top-to-the-W to NW sense of shear (Wallis and Behrmann, 1996).

Garnet growth took place during Cretaceous Barrovian-type metamorphism. The presence of the assemblage biotite + kyanite + staurolite + garnet (Fig. 7a in Wallis and Behrmann (1996)) suggests minimum metamorphic conditions of around 7 kbar and 630 °C (Spear and Cheney, 1989). Under these conditions crystal plasticity is likely to be the dominant deformation mechanism in quartz-rich rocks and this is supported by the presence of D_r quartz crystallographic preferred orientation patterns.

3.2. Microstructure

The mineral assemblage of the pelitic sample #80904 is garnet + biotite + muscovite + chlorite + plagioclase + quartz + ilmenite + graphite, and is consistent with the garnet-forming reaction given by Eq. (1). Preferred orientation of muscovite and biotite defines the foliations (S_1 and S_2) in this sample. Crenulation of S_1 formed during the second phase of deformation produces a compositional banding composed of millimetre-scale mica-rich and -poor layers. A crenulation lineation related to a later stage of deformation is also recognised on the S_2 surface. A thin section was prepared perpendicular to both S_1 and S_2. In this plane, most garnet grains have clear spiral trails of inclusions, suggesting that the two-fold symmetry axis of most grains is perpendicular to the section. The horizontal direction of the photomicrograph shown in Fig. 1a corresponds to the direction of the strike of S_1 (N35°W). Foliations S_1 and S_2 are roughly horizontal and vertical, respectively.

The spiral arms of the garnet grain shown in Fig. 1a are symmetrical. They are in contact with the grains of muscovite and biotite comprising S_1, suggesting that the arms grew together with biotite at the expense of the S_1 muscovite through reaction (1) and that the growth was controlled by diffusion in the matrix. Some S_1 biotite grains are partially included at the margin of the garnet grain (Fig. 1a). These indicate that garnet growth occurred both during and after

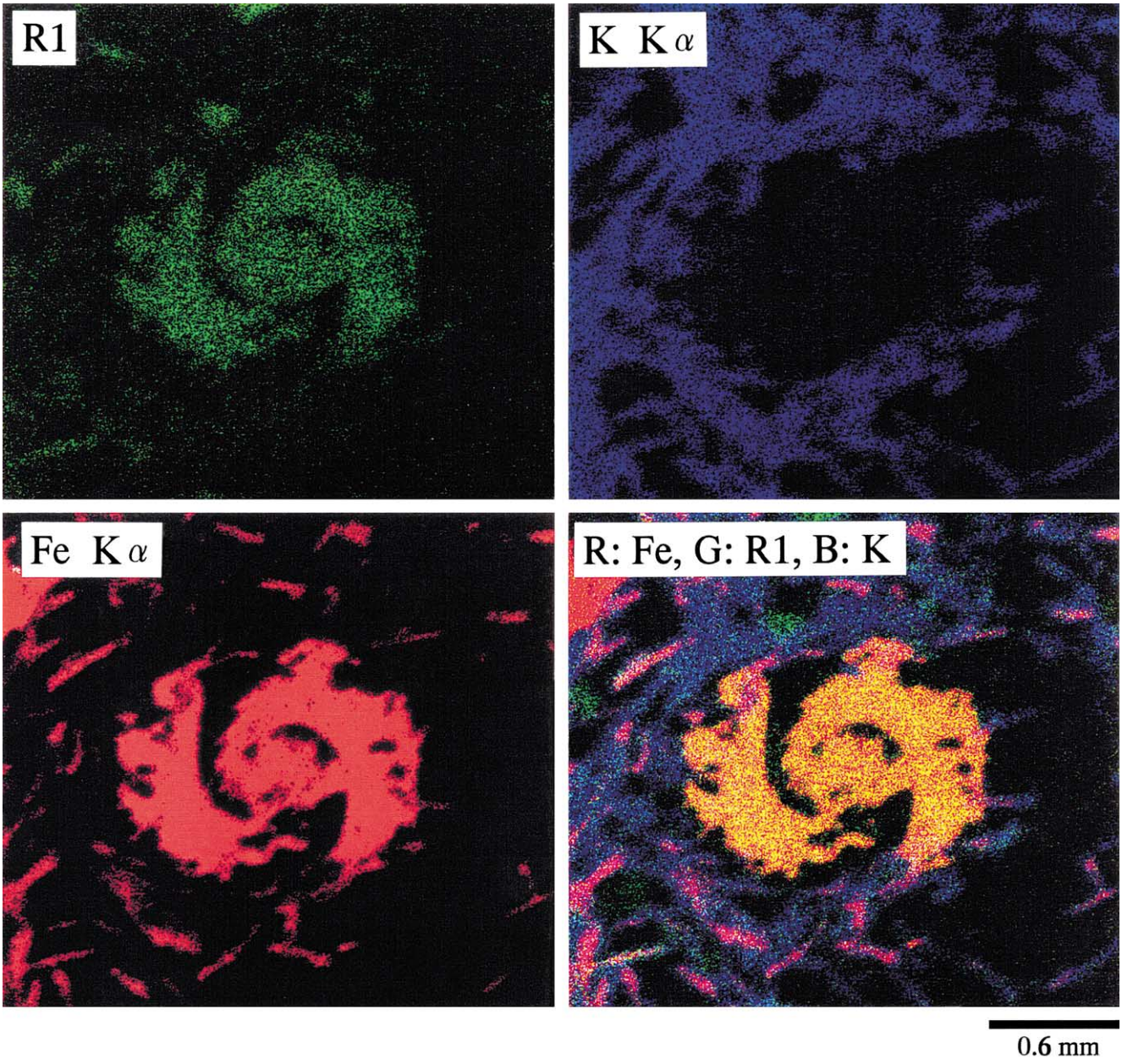

Fig. 2. X-ray image maps of the sample #80904 for the {842} reflection (R_1) and Kα lines of K and Fe of the garnet and the summation of the three lines. The garnet grain is identical to that in the centre of Fig. 1a.

the first phase of deformation. The inclusion trails within the garnet grain are therefore a continuation of S_1, as described by Treagus (1974). Fine-grained elongate inclusions of quartz and ilmenite occur completely within the garnet grain (top centre of Fig. 1b). In contrast, coarser and less ellipsoidal quartz grains lie between the spiral arms of the garnet, where skeletal garnet grew along quartz grain boundaries, partially enclosing the quartz grains. The traces of long axes of the former inclusion grains have a tightly spiral shape, whereas those of the latter grains are less curved. The boundary between the domains containing these two types of inclusions is geometrically analogous to the truncation plane of Bell and Johnson (1989). The skeletal branches of garnet intervening spiral arms are curved, i.e. upward convex at the right-hand side of Fig. 1b and downward convex at the left-hand side. These curvatures are similar to those of included foliations that are originally located at the strain shadow by the rotational model of Schoneveld (1977).

The sample #MS95 contains garnet, biotite, amphibole, muscovite and quartz together with minor calcite, plagioclase and secondary chlorite. The sample was cut perpendicular to the foliation and in a direction parallel to the dominant stretching lineation (Fig. 1c). Garnet in this sample is ovoidal and is not composed of spiral arms with intervening skeletal parts. Most grains of quartz and

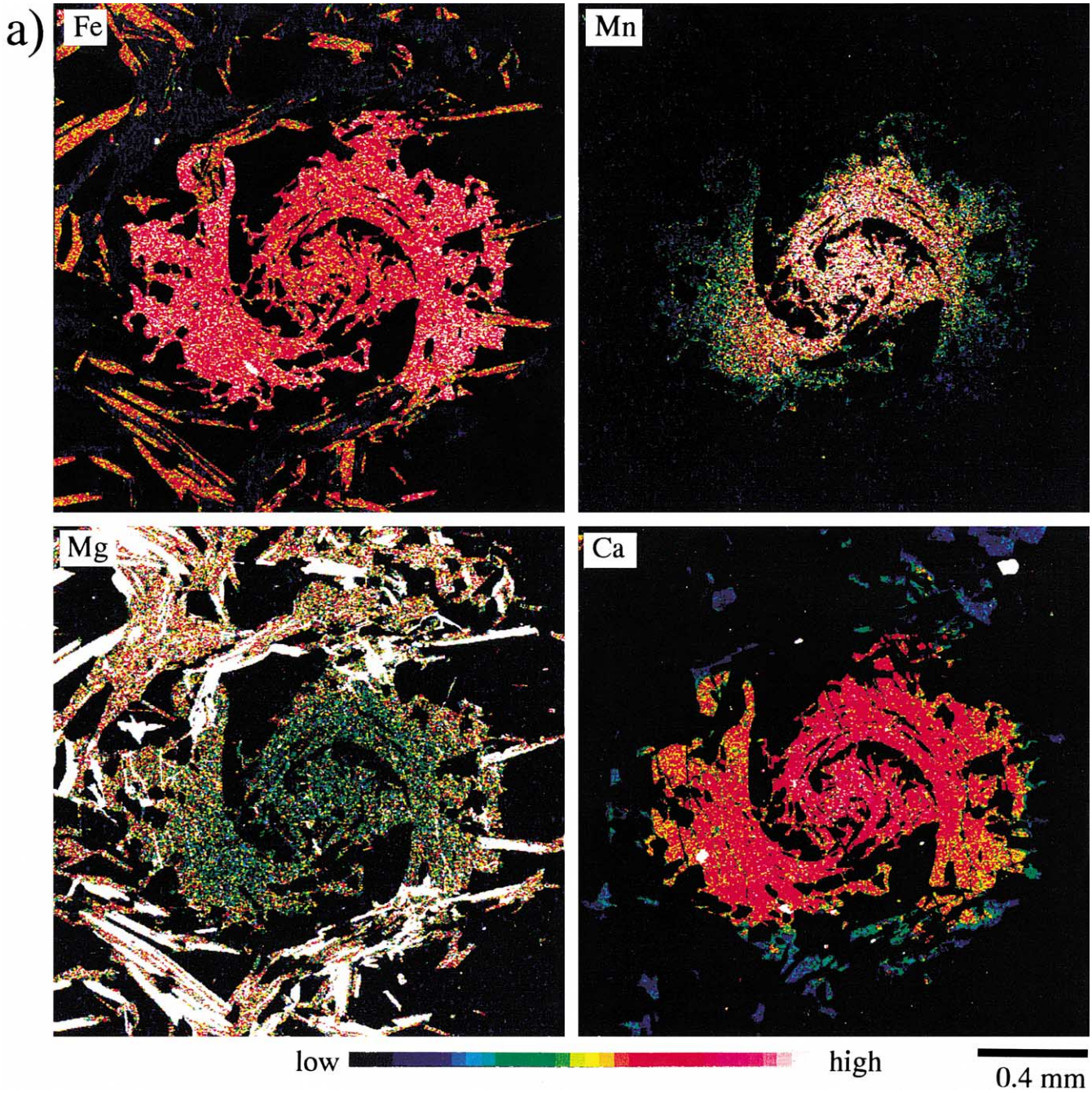

Fig. 3. X-ray image maps with respect to Fe, Mn, Mg and Ca. Grains of garnet in (a) and (b) are identical to those in Fig. 1a and c, respectively.

ilmenite are completely included in garnet. In spite of such differences in the mode of occurrence, the garnet of sample #MS95 also contains spiral and less curved inclusion trails (Fig. 1d). The spiral fabrics within the garnet are a continuation of the S_r foliation (see above) although the dominant mesoscopic fabric in this sample is in fact S_s (see also Fig. 7b of Wallis and Behrmann (1996)). Coarse garnet (<2 mm) is common in the sample and, in general, different grains show very similar spiral features with two-fold symmetry axes approximately perpendicular to the section surface. However, locally, the inclusion trail patterns of the garnet suggest the spiral axis is oriented obliquely to the section surface. This variation in the orientation of the spiral axes may be explained by Ds deformation that postdates garnet growth.

3.3. Crystallographic orientation

For the grain shown in Fig. 1a, an X-ray diffraction peak was detected with ca. 5.16 keV in the energy-dispersive spectrum when the beam was focused on a point of garnet grain at $\chi = +2°$ and $\phi = 0°$. This peak can be attributed to

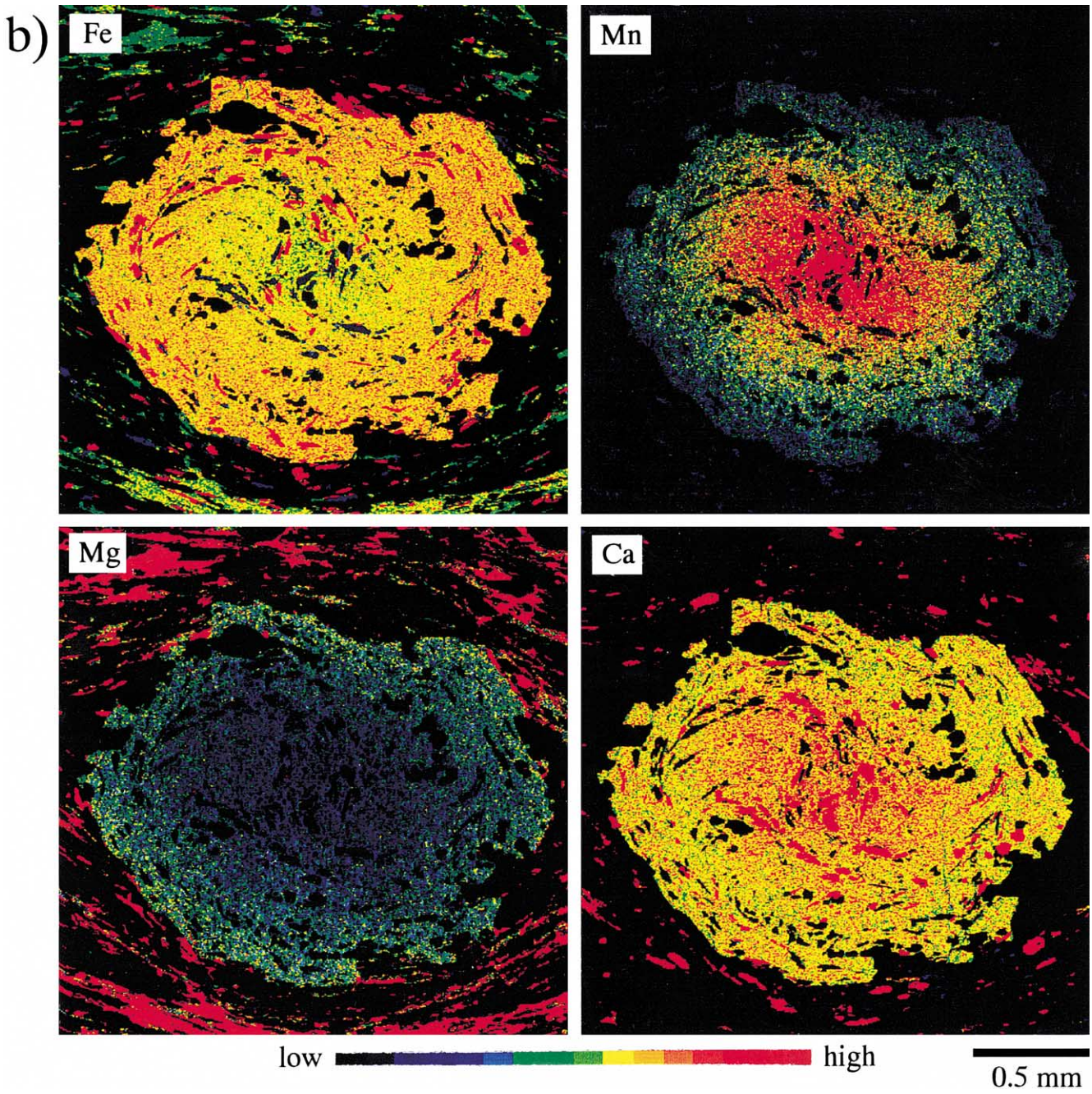

Fig. 3. (*continued*)

diffraction by {842} planes. We then set an energy range between 4.98 and 5.32 keV as R_1 and by scanning the sample we obtained maps of both crystallographic orientation and element distribution. Fig. 2 shows the crystallographic orientation map and two element maps for K and Fe, respectively. A map for R_1 shown in Fig. 2 shows that the whole of the sigmoidal grain of garnet is uniformly coloured, indicating that every part of this garnet grain has the same crystallographic orientation. The degree of angular mismatch in crystallographic orientation that can be recognised depends on the working distance used in the measurement. A working distance of 3 mm was used to detect the X-ray intense enough to construct Fig. 2. In this case it is not possible to recognise differences in crystallographic orientation of less than 4°. To check the significance of these results we also studied the sample using a working distance of 20 mm, which enable us to recognise 1° differences in crystallographic orientation, despite the low X-ray intensity and the low resolution (X-ray beam: 100 μm in diameter). In both cases a uniform reflection pattern indicated no crystallographic mismatch across the grain.

In addition to the garnet of this study, several other grains

Table 1
Representative analyses of constituent minerals of sample #80904

Mineral	Biotite	Muscovite	Chlorite	Plagioclase	Ilmenite	Garnet	
Analysed point	Bt-12	Ms-1	Chl-1	Pl-1	Ilm-3	Grt-93 rim	Grt-36 core
SiO_2	35.33	47.28	27.92	64.54	0.45	37.11	37.15
TiO_2	2.16	0.52			52.11		
Al_2O_3	17.41	31.34	19.50	22.42		20.55	21.00
FeO	25.61	2.93	31.32	0.21	43.49	34.20	27.80
MnO					4.24	0.36	5.39
MgO	6.39	1.47	8.28			1.06	0.53
CaO				3.28	0.14	6.47	8.63
Na_2O	0.74	0.84	0.83	10.21			
K_2O	8.99	10.21	3.09	0.14			
Total	96.63	94.59	90.94	100.80	100.43	99.75	100.50
Si	5.470	6.392	5.939	2.831	0.045	3.010	2.986
Ti	0.252	0.053			3.939		
Al	3.177	4.994	4.889	1.159		1.964	1.990
Fe	3.316	0.331	5.572	0.008	3.655	2.320	1.869
Mn					0.361	0.025	0.367
Mg	1.475	0.296	2.626			0.128	0.064
Ca				0.154	0.015	0.562	0.743
Na	0.222	0.220	0.342	0.868			
K	1.776	1.761	0.839	0.008			
O =	22	22	28	8	12	12	12

also show a high contrast in the map for R_1 (Fig. 2). This is due to a chance coincidence in the direction of diffracted X-rays from the garnet and other minerals. Superposing the three images related to both composition and crystallographic orientation allows the different grains to be distinguished (RGB image in Fig. 2). Only the garnet grain is coloured yellow. In contrast, biotite grains are purple. The orientation maps using different diffracted X-rays (e.g. {1042}, {642} and {1222} reflections at different $\chi-\phi$ conditions) also show that the whole region of the sigmoidal grain has the same crystallographic orientation. Consequently, we concluded that the sigmoidal garnet grain was composed of a single crystal in spite of its complex shape. The same technique applied to the grain of the sample #MS95 shown in Fig. 1c confirmed that this was also composed of a single crystal with no evidence of subgrain formation.

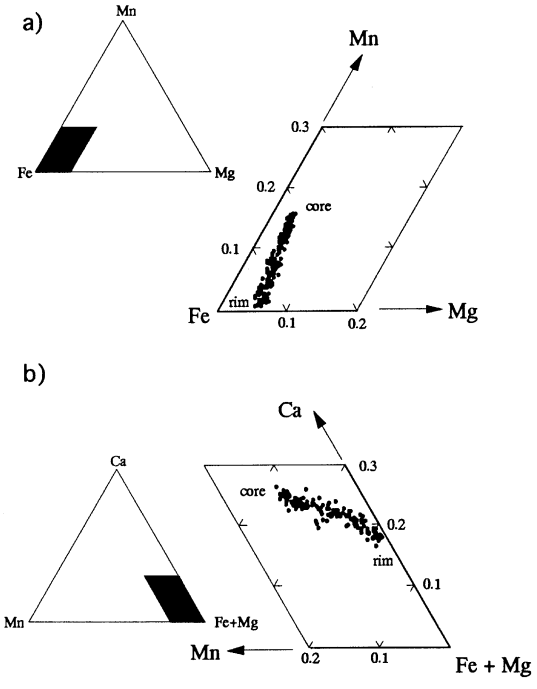

Fig. 4. Chemical composition of garnet from the sample #80904. (a) Fe–Mg–Mn ratio; (b) Mn–(Fe + Mg)–Ca ratio.

3.4. Mineral composition

Qualitative chemical zoning profiles with respect to Fe, Mn, Mg and Ca of the garnet grains of Fig. 1a and c are shown in Fig. 3a and b, respectively. Garnet grains from both samples show an increase in Mg and decreases in Mn and Ca from the core towards the periphery. Each grain shows a single maximum in the Mn content. Enrichment of the spessartine component at the margin is not recognised. The chemical zoning of both grains is continuous except for the upper-left and lower-right parts of the grain in Fig. 3a, where a possible chemical discontinuity exists. The region where a deflection of the inclusion trails is recognised does not coincide geometrically with the location where a chemical discontinuity may be present. The shapes of described contours in chemical composition are not circular but approximately ellipsoidal and oriented obliquely to the slightly ellipsoidal shape of grain. In both samples, the long and short axes of the contour ellipses

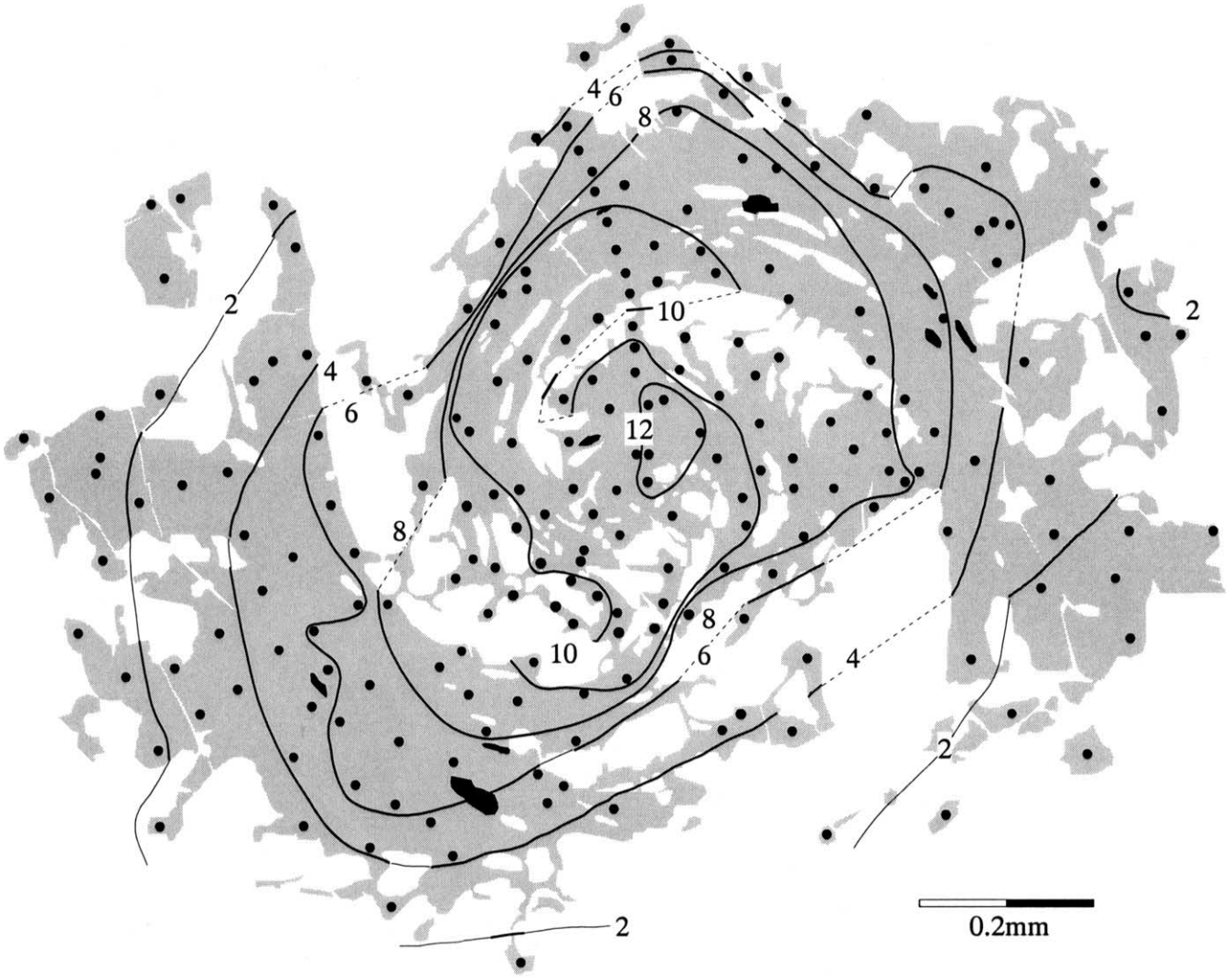

Fig. 5. Chemical contour map of the same garnet grain as shown in Fig. 3a. The lines are defined by quantitative analyses of the points shown as solid dots. Numbers denote the spessartine content of the contour line in mol%. Open and solid inclusions are quartz and ilmenite, respectively. Note that the long axes of the shape encompassed by the contours rotate clockwise with descending spessartine content and that the contour of 10 mol% spessartine shows the development of two spiral arms.

show relative rotations with increasing diameter that are compatible with the sense of curvature shown by the inclusion trails (Fig. 3a and b).

Quantitative chemical analyses of the sample #80904 allow these features to be defined more precisely. Constituent minerals other than garnet are chemically homogeneous within the section, and their representative analyses are shown in Table 1. The spessartine content decreases from 12 mol% at the centre to nearly zero at the periphery (Fig. 4). In total, analyses of 180 points were used to define the chemical contour lines for the spessartine component of the garnet (Fig. 5). The chemical contours are neither parallel nor perpendicular to the direction of the spiral arms of the garnet grain. The shape encompassed by the contour line of 10 mol% of spessartine content has two spiral arms. Similar shapes of contours are obtained if other endmembers of garnet are used to produce chemical maps.

Fig. 6 plots the long axes of the contour shapes as a function of the angle made with the matrix schistosity, S_1. The results show that the long axis rotates clockwise some 40° during the chemical interval between 10 and 4 mol% of spessartine. During the same growth interval, inclusion trails show a change in orientation of about 90°. For a given change in spessartine content the angular changes in both inclusion trails and the long axis of the contour decrease with increasing diameter.

3.5. Three-dimensional geometry

Fig. 7 shows successive CT images, which focuses on a single garnet grain of the sample #80904. The images are arranged in order of increasing distance from the viewpoint, with a spacing between the images of 75.9 μm. The

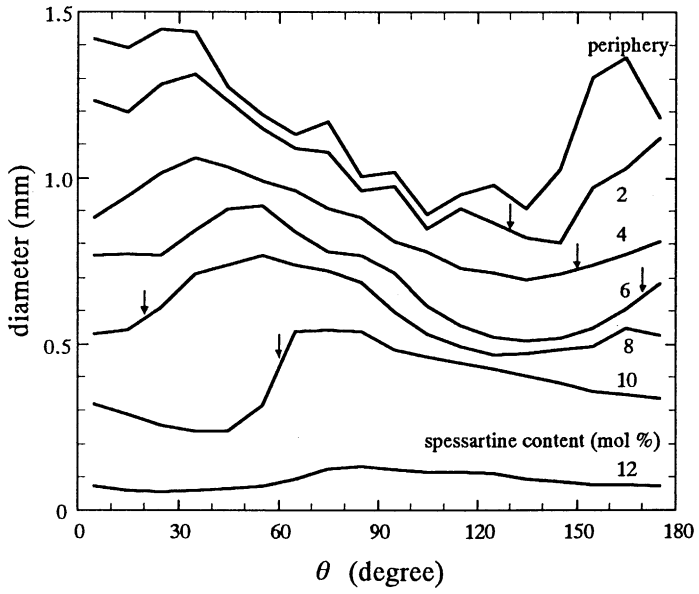

Fig. 6. Diameters of the shape encompassed by the chemical contours of garnet grain in Fig. 5 as a function of the angle from the external schistosity S_1, θ, which is measured anticlockwise. The arrows show the approximate portions in which the garnet grain incorporates coarser and less ellipsoidal quartz grains.

orientation of the image is the same as Fig. 1a, i.e. the schistosity (S_1) of the sample lies horizontal.

The differences in brightness are related to the X-ray attenuation of minerals. Objects with high and low brightnesses correspond to those with high and low linear attenuation coefficients (LAC), respectively. Because the LAC value is a function of the photon energy of the incoming X-ray beam and in the present study, a polychromatic X-ray beam was used, we used an olivine crystal from San Carlos, USA (SCO = San Carlos olivine: $Fo_{91.8}$) as a standard to quantitatively evaluate the CT value, which is a quantitative expression of the brightness in a CT image (Tsuchiyama et al., 2002). The range of the CT values, which were normalised by those of SCO and air (defined as 100 OU for SCO and 0 OU for air: OU = olivine unit), was adopted from 39.5 to 224 OU in Fig. 7 to show better contrast among the minerals.

The LAC values of the minerals in the present specimen can be calculated from the chemical compositions (Table 1) and the densities as a function of the photon energy (e.g. Tsuchiyama et al., 2000). The densities of the minerals were estimated from the reference values of endmembers for minerals (Olhoeft and Johnson, 1989) by assuming that Vegard's law can be applied to garnet and plagioclase. The normalised LAC values are 211, 133, 85.0, 67.2, 66.9 and 356 OU at 60 kV for garnet, biotite, muscovite,

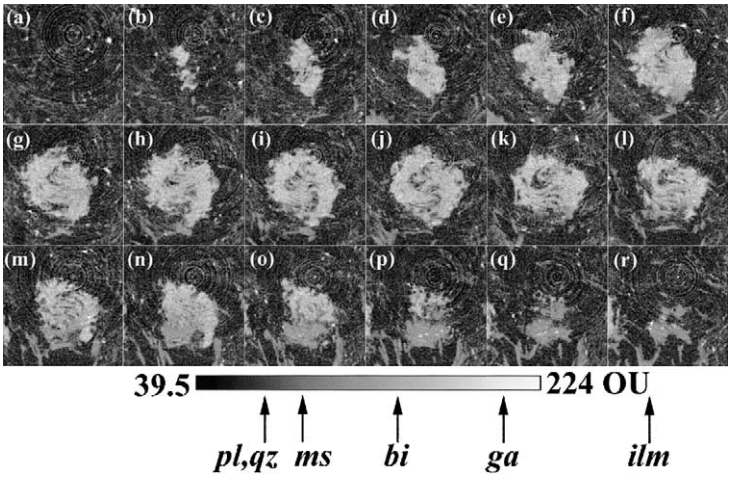

Fig. 7. Successive CT images of a sigmoidal garnet from sample #80904 for every nine slice intervals (75.9 μm interval). The width and height of each CT image is 1.90 mm. The range of normalised CT values showing each image is from 39.5 to 224 OU. The CT values expected for plagioclase (pl), quartz (qz), muscovite (ms), biotite (bi), garnet (ga) and ilmenite (ilm) are also shown together with a grey scale. The CT value for ilmenite is out of scale. See text for more details.

plagioclase, quartz and ilmenite, respectively. Chlorite has a LAC value similar to biotite. The garnet LAC value is almost constant within the compositional range of the zoning. If the calibrated relation between the normalised LAC and CT values for the present CT scanner obtained by Tsuchiyama et al. (2002) was used, the normalised CT values expected for the minerals would be 180, 130, 85, 67, 67 and 250 OU, respectively. They are shown with a grey scale in Fig. 7.

The bright object at the centres of Fig. 7b–q is garnet. Small objects slightly darker than garnet in the matrix are biotite. Large objects below the garnet grain (Fig. 7m–r) are also biotite. Quartz, plagioclase, and muscovite are imaged as dark matrix. Quartz and plagioclase cannot be distinguished from each other because their LAC values are almost the same. Slightly brighter portions in the matrix are muscovite. The concentric rings observed in the figure are imaging artifacts superimposed on the CT images. This ring artifact is mainly caused by time drift of the X-ray detector elements during the data acquisition.

The successive images of the whole garnet grain shows that the height of the grain is about 1.2 mm, which is similar to its width. The image with the maximum width is Fig. 7i suggesting that this represents a section passing very close to the centre of the garnet. Although the spatial resolution still has room for improvement, the images allow the general geometry of the quartz inclusion trails within the garnet to be discerned. In Fig. 7i, the spiral shape of the garnet grain can be seen and it has arms that curve with a clockwise sense and decreasing curvature with increasing distance from the centre of the grain. The arms at the 3-D centre of the grain (Fig. 7i) are inclined anticlockwise ca. 50° with respect to the schistosity, S_1. In contrast, the arms that pass through the upper or lower portions of the grain have distinct orientations. The orientations of the arms passing through the two-dimensional centres are almost parallel to S_1 in Fig. 7f and m. The change in orientation of the arms seems to be continuous even with an image spacing as small as 75.9 μm. Significant features analogous to truncation planes of Bell and Johnson (1989) were not detected. The changes in the geometry of the arms in successive images suggest that the arms or inclusion trails have a complex non-cylindrical 3-D shape with tighter curvature near the centre of the grain. This type of geometry is consistent with the 3-D structures of the twisting inclusion trails described by Powell and Treagus (1967, 1970) and Johnson (1993). The pattern of inclusion trails maintains good two-fold symmetry throughout the sections, suggesting that the orientation of the symmetry axis (rotation axis or FIA) of the grain is almost perpendicular to the images.

4. Discussion

The orientation of the symmetry axis of the garnet grain shown in Fig. 7 is approximately parallel to the intersection of S_1 and S_2 in Fig. 1a, i.e. parallel to the intersection of two highly oblique foliations. This configuration can be explained by both the rotational and non-rotational models, as suggested by Bell et al. (1995). However, the complex but regular involute spiral shape of the inclusion trails revealed by the CT scanning is best explained by a rotational model. In non-rotational models, the orientation of inclusion trails should change discontinuously in the direction of two-fold symmetry axis, as well as in radial directions perpendicular to this axis. In this section we examine the chemical zoning and microstructures described above to further test which of the two models is most plausible.

The pyrope content of garnet produced by reaction (1) increases with ascending metamorphic temperature. The composition of matrix biotite and that of the periphery of the garnet grain with maximum pyrope content may provide a peak metamorphic temperature of the sample #80904, which is 470 °C using the geothermometer of Ferry and Spear (1978) at a pressure of 6 kbar. Using the method of Dasgupta et al. (1991) gives an estimated 10 °C lower than that of Ferry and Spear (1978). These temperatures are insufficient to modify the growth zoning of garnet effectively by volume diffusion (e.g. Yardley, 1977; Dempster, 1985; Ikeda, 1993). The consistent crystallographic orientation and the presence of a single Mn maximum within any grain indicate that the shape of the sigmoidal grain is due to nucleation in one place and subsequent overgrowth on it. None of the processes of plastic deformation, impingement of multiple grains or brittle fracturing followed by crack-filling can explain the sigmoidal shape. The lack of a zone with Mn enrichment suggests that no resorption of garnet took place during and after growth of garnet. We can, therefore, regard the chemical contours as representing the grain shapes during growth. The chemical zoning of garnet shown in Fig. 5 suggests the following aspects of the growth history.

First, the continuous growth zoning preserved in garnet grain indicates that the continuous garnet growth took place through a single increase in metamorphic grade, i.e. a single metamorphic event. It is difficult to produce such chemical zonings of garnet by discrete multiple stages of garnet growth as is required by the non-rotational model. Second, a single chemical contour representing a growth surface envelops quartz grains with distinctly different orientations (e.g. 8 and 10 mol% spessartine contours in Fig. 5). This suggests that 'truncation zones' such as that shown in Fig. 1 are formed by the simultaneous incorporation of distinctly oriented quartz grains. The coarser grains may originally have formed in strain shadows around the garnet as suggested by Schoneveld (1977). Third, during part of its growth the garnet grain had a clear spiral morphology as shown by the shape of the 10 mol% spessartine contour (Fig. 5). A radial trace across the garnet, therefore, gives us no clear information about the temporal sequence of either the incorporation of minerals or the orientation of

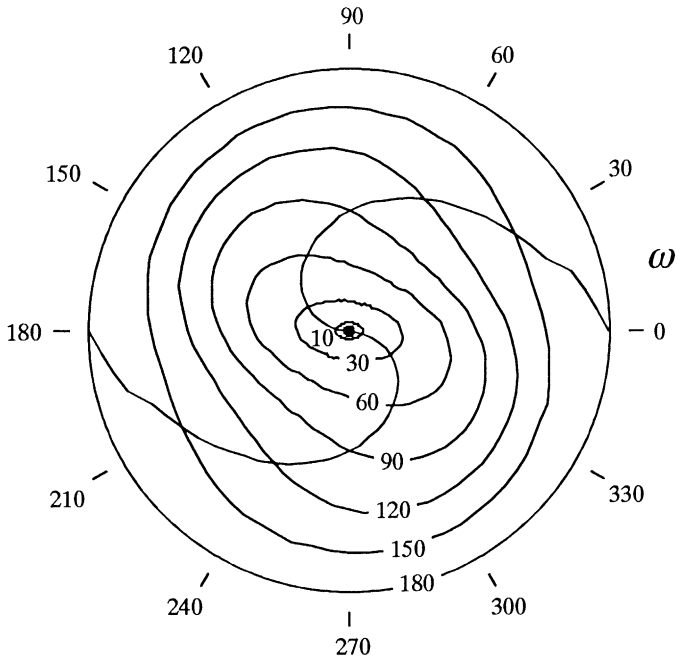

Fig. 8. Progressive changes in shape and orientation of a rotating grain undergoing anisotropic growth on a spherical nucleus during anticlockwise rotation. The amount of incremental increase in radius is given by Eq. (2) as a function of the angle from the mica-rich portion, ω. The grains are arranged so that their nuclei have an identical orientation that is 180° from the initial starting position. The numbers denote the rotation angle through which the core of the grain had rotated when the encompassing grain was formed. The sigmoidal lines emanating from the centre represent the trace of the portion of the maximum growth rate.

external foliation with respect to the garnet. Finally, the long axis of the grain has rotated during its growth, in the same direction as the inclusion trails, but to a lesser degree (Fig. 6). The difference in behaviour between the change in orientation of the shape of the grain and the orientation of the inclusion trails is a puzzling feature not readily explained by either the rotational or non-rotational models. The non-rotational model for the general development of porphyroblasts (e.g. Bell and Johnson, 1989) invokes a series of stages with horizontal and vertical foliations roughly perpendicular to one another. Even though the model does not deal with the anisotropic growth, it is expected that the direction of the maximum growth rate is largely controlled either by the presence of micas suitable for the garnet-producing reaction or by growth in a non-hydrostatic stress field. Orthogonal changes in the stress field will bring about orthogonal changes not only in the orientation of foliation, but also in the direction of the maximum growth rate, which is inconsistent with the observed features in the present work. The observed changes in shape of the garnet and orientation of inclusion trails are, however, compatible with a rotational model as outlined below.

We consider a growing grain of garnet that is simultaneously rotating anticlockwise with respect to a reference frame attached to the external foliation. We also assume that the direction of the maximum growth rate is parallel to the foliation. Once incorporated into the grain, the inclusions undergo rigid-body rotation and their orientation gives a measure of the true rotation of the grain. In contrast the long axes of the growing grain rotate to a lesser degree because the maximum incremental growth direction is maintained in a direction parallel to the foliation. A simple calculation represents this phenomenon semi-quantitatively. Consider anisotropic growth on a spherical nucleus during anticlockwise rotation. The incremental growth of the radius per incremental rotation, Δr, is assumed to be time-independent and a function of the angle from the direction of the maximum growth rate, ω, such that the increment produces an ellipse of the form:

$$\Delta r(\omega) = \sqrt{\frac{a^2 b^2}{a^2 \sin^2\omega + b^2 \cos^2\omega}} \tag{2}$$

where a and b denote the lengths of the long and short axes of the ellipse, respectively. Parameters Δr, a and b are normalised by the radius of the grain after 180° rotation, i.e. they all have dimensions of degree^{-1}. We can then calculate the shape and orientation of the grains as a function of the rotation angle of their nuclei. All the shapes encompassed by the contours shown in Fig. 5 possess an identical nucleus that are rotated through a specific angle. In order to compare the theoretical results with Fig. 5, all the calculated shapes are shown after a 180° rotation of the core. One such example is shown in Fig. 8 where values of 0.8 and 0.4 are used for a and b, respectively. The numbers represent the full rigid body rotations of the core. In this example it can be seen that the long axis of the grain only

rotates 70° when the grain has undergone a full rotation of 180°.

Whether or not they include the anisotropic growth feature discussed above, all rotational models predict a complex non-coaxial twisting feature of the inclusion trails related by a centre of symmetry and a two-fold rotation axis (Powell and Treagus, 1970; Schoneveld, 1977). The CT images of this study suggest that the inclusion trails of the garnet in this study have a complex involute spiral geometry (Fig. 7). This result is consistent with the rotational model proposed in this study.

The present calculation gives a semi-quantitative explanation of the observed geometrical features of garnet; however, it should be noted that the calculation does not consider change in the rotation rate of the grains. In general, such changes are expected for non-spherical grains suspended in a viscous matrix undergoing non-coaxial flow (Jeffery, 1922; Powell and MacQueen, 1976; Masuda et al., 1995). When deformation is simple shear, the rate of rotation will be minimum when the long axis of the ellipsoidal grain is parallel to the shear plane and shear direction, which at high strains will be subparallel to the stretching lineation. This will enhance the anisotropic growth described by Eq. (2) and may increase the angular difference between the true relative rotation and the long axis rotation. The above calculation also does not include movement of the material in the vicinity of the garnet grain due to viscous flow, which is examined theoretically by Masuda and Ando (1988) and Gray and Busa (1994). In contrast, Rosenfeld (1970) proposes a simple model, referred to as ring model, in which the grain growing isotropically rotates and incorporates inclusion minerals occurring within a fixed plane. Gray and Busa (1994) show that the ring model is applicable if the rotation angle is less than 180°, suggesting that the effect of not considering the movement of the material around garnet is negligible. The mica-rich portion is ca. 120° from the schistosity S_1 (Fig. 1a). Rotating Fig. 8 anticlockwise ca. 120° may also explain the vertically-oriented long axis of the shape at the early stage. Despite the simplification, the present model can well explain the observed phenomenon that the long axis rotates less than the grain.

5. Conclusions

Sigmoidal garnets from two separate samples are single crystals, showing that significant ductile or brittle deformation is not required to form them and also that they are not the result of the amalgamation of independent grains.

Chemical mapping of sigmoidal garnets is continuous with no clear breaks suggesting that they grew during a single metamorphic event. Detailed chemical mapping also reveals that the garnet grew in elongate, approximately ellipsoidal, shapes. The long axis of individual growth ellipsoids do not coincide but show an angular displacement. This displacement has the same sense as that of the curvature of the internal fabric of the garnet. These features are best explained as continuous syn-growth rotation of the garnet with respect to the maximum growth direction of the garnet. Non-rotational models for the formation of sigmoidal garnet would suggest a much more complex pattern with sudden changes between different growth stages.

CT scanning of sigmoidal garnet can successfully reveal the main features of the 3-D shape of the inclusion trails and orientation of the symmetry axis without cutting the sample. The results of this study show that the spiral arms have a complex 3-D spiral geometry. This type of geometry is consistent with twisting features predicted by rotational models for the formation of sigmoidal garnets.

Acknowledgements

T. Ikeda is grateful to T. Masuda of Shizuoka University for valued comments. S. Nakano of Shiga University is acknowledged for his experimental assistance with the microanalyser. The authors express their appreciation to R. Trouw, J. Mezger and C.W. Passchier for their constructive comments that helped improve this manuscript. This work was financially supported in part by Grants-in-Aid for Scientific Research (A) (11304035) and (C) (11640482) from the Japan Society for the Promotion of Science.

References

Aerden, D.G.A.M., 1995. Porphyroblast non-rotation during crustal extension in the Variscan Lys–Caillaouas Massif, Pyrenees. Journal of Structural Geology 17, 709–725.

Bailey, E.B., 1923. The metamorphism of the South-west Highlands. Geological Magazine 60, 317–331.

Bailey, E.B., Maufe, H.B., 1960. The Geology of Ben Nevis and Glen Coe, and the surrounding country (explanation of Geological Sheet 53). Memoirs of the Geological Survey of Great Britain, Scotland.

Bass, J.D., 1995. Elasticity of minerals, glasses, and melts. In: Ahrens, T.J. (Ed.), Mineral Physics and Crystallography: a Handbook of Physical Constants. American Geophysical Union Reference Shelf 2, pp. 45–63.

Bell, T.H., Johnson, S.E., 1989. Porphyroblast inclusion trails: the key to orogenesis. Journal of Metamorphic Geology 7, 279–310.

Bell, T.H., Hickey, K.A., 1997. Distribution of pre-folding linear indicators of movement direction around the Spring Hill Synform, Vermont: significance for mechanism of folding in this portion of the Appalachians. Tectonophysics 274, 275–294.

Bell, T.H., Mares, V.M., 1999. Correlating deformation and metamorphism around orogenic arcs. American Mineralogist 84, 1727–1740.

Bell, T.H., Johnson, S.E., Davis, B., Forde, A., Hayward, N., Wilkins, C., 1992. Porphyroblast inclusion-trail orientation data: epuure non son girate! Journal of Metamorphic Geology 10, 295–307.

Bell, T.H., Forde, A., Wang, J., 1995. A new indicator of movement direction during orogenesis: measurement technique and application to the Alps. Terra Nova 7, 500–508.

Bell, T.H., Hickey, K.A., Wang, J., 1997. Spiral and staircase inclusion trail axes within garnet and staurolite porphyroblasts from schists of the Bolton Syncline, Connecticut: timing of porphyroblast growth and the effects of fold development. Journal of Metamorphic Geology 15, 467–478.

Bell, T.H., Hickey, K.A., Upton, J.G., 1998. Distinguishing and correlating multiple phases of metamorphism across a multiply deformed region using the axes of spiral, staircase and sigmoidal inclusion trails in garnet. Journal of Metamorphic Geology 16, 767–794.

Dalziel, I.W.D., Bailey, S.W., 1968. Deformed garnets in a mylonitic rock from the Grenville front and their tectonic significance. American Journal of Science 266, 542–562.

Dasgupta, S., Sengupta, P., Guha, D., Fukuoka, M., 1991. A refined garnet–biotite Fe–Mg exchange geothermometer and its application in amphibolites and granulites. Contributions to Mineralogy and Petrology 109, 130–137.

Dempster, T.J., 1985. Garnet zoning and metamorphism of the Barrovian type area, Scotland. Contributions to Mineralogy and Petrology 89, 30–38.

Denison, C., Carlson, W.D., Ketcham, R.A., 1997. Three-dimensional quantitative textural analysis of metamorphic rocks using high-resolution computed X-ray tomography: Part I. Methods and techniques. Journal of Metamorphic Geology 15, 29–44.

Ferry, J.M., Spear, F.S., 1978. Experimental calibration of the partitioning of Fe and Mg between biotite and garnet. Contributions to Mineralogy and Petrology 66, 113–117.

Gray, N.H., Busa, M.D., 1994. The three-dimensional geometry of simulated porphyroblast inclusion trails: inert-marker, viscous-flow models. Journal of Metamorphic Geology 12, 575–587.

Hayward, N., 1992. Microstructural analysis of the classical spiral garnet porphyroblasts of south-east Vermont: evidence for non-rotation. Journal of Metamorphic Geology 10, 567–587.

Hickey, K.A., Bell, T.H., 1999. Behaviour of rigid objects during deformation and metamorphism: a test using schists from the Bolton syncline, Connecticut, USA. Journal of Metamorphic Geology 17, 211–228.

Ikeda, T., 1993. Compositional zoning patterns of garnet during prograde metamorphism from the Yanai district, Ryoke metamorphic belt, southwest Japan. Lithos 30, 109–121.

Ikeda, T., 1996. Structural analysis of the Dalradian rocks of the Loch Leven area, Inverness-shire. Scottish Journal of Geology 32, 179–184.

Jeffery, G.B., 1922. The motion of ellipsoidal particles immersed in a viscous fluid. Proceedings of Royal Society of London Series A 102, 161–179.

Ji, S., Martignole, J., 1994. Ductility of garnet as an indicator of extremely high temperature deformation. Journal of Structural Geology 16, 985–996.

Ji, S., Zhao, P., Saruwatari, K., 1997. Fracturing of garnet crystals in anisotropic metamorphic rocks during uplift. Journal of Structural Geology 19, 603–620.

Johnson, S.E., 1990. Lack of porphyroblast rotation in the Otago schists, New Zealand: implications for crenulation cleavage development, folding and deformation partitioning. Journal of Metamorphic Geology 8, 13–30.

Johnson, S.E., 1993. Unravelling the spirals: a serial thin-section study and three-dimensional computer-aided reconstruction of spiral-shaped inclusion trails in garnet porphyroblasts. Journal of Metamorphic Geology 11, 621–634.

Kamineni, D.C., 1978. A study of some garnet aggregates from Yellowknife, Canada. Neues Jahrbuch fur Mineralogie Monatshefte 10, 455–462.

Karato, S., 1989. Plasticity–crystal structure systematics in dense oxides and its implications for the creep strength of the Earth's deep interior: a preliminary result. Physics of the Earth and Planetary Interiors 55, 234–240.

Masuda, T., Ando, S., 1988. Viscous flow around a rigid spherical body: a hydrodynamical approach. Tectonophysics 148, 337–346.

Masuda, T., Michibayashi, K., Ohta, H., 1995. Shape preferred orientation of rigid particles in a viscous matrix: re-evaluation to determine kinematic parameters of ductile deformation. Journal of Structural Geology 17, 115–129.

Olhoeft, G.R., Johnson, G.R., 1989. Densities of rocks and minerals. In: Carmichael, R.S. (Ed.). Practice Handbook of Physical Properties of Rocks and Minerals. CRC Press, Boca Raton, FL, pp. 141–176.

Passchier, C.W., Trouw, R.A.J., Zwart, H.J., Vissers, L.M., 1992. Porphyroblast rotation: eppur si muove? Journal of Metamorphic Geology 10, 283–294.

Pattison, D.R.M., 1989. $P–T$ conditions and the influence of graphite on pelitic phase relations in the Ballachulish aureole, Scotland. Journal of Petrology 30, 1219–1244.

Pattison, D.R.M., Voll, G., 1991. Regional geology of the Ballachulish area. In: Voll, G., Topel, J., Pattison, D.R.M., Seifert, F. (Eds.). Equilibrium and Kinetics in Contact Metamorphism. Springer-Verlag, Berlin, Heidelberg, pp. 19–36.

Powell, D., Treagus, J.E., 1967. On the geometry of S-shaped inclusion in garnet porphyroblasts. Mineralogical Magazine 36, 453–456.

Powell, D., Treagus, J.E., 1970. Rotational fabrics in metamorphic minerals. Mineralogical Magazine 37, 801–814.

Powell, D., MacQueen, J.A., 1976. Relationships between garnet shape, rotational inclusion fabrics and strain in some Moine metamorphic rocks of Skye, Scotland. Tectonophysics 35, 391–402.

Richardson, S.W., Powell, R., 1976. Thermal causes of the Dalradian metamorphism in the central Highlands of Scotland. Scottish Journal of Geology 12, 237–268.

Rosenfeld, J.L., 1970. Rotated garnets in metamorphic rocks. Geological Society of America Special Paper 129.

Schoneveld, C., 1977. A study of some typical inclusion patterns in strongly paracrystalline-rotated garnets. Tectonophysics 39, 453–471.

Shimobayashi, N., Minato, J., Kitamura, M., 1999. Application of an X-ray analytical microscope to the study of polycrystallines. Earth and Planetary Science using Synchrotron Radiation, KEK Proceedings 99-14, pp. 83–86.

Spear, F.S., 1993. Metamorphic phase equilibria and pressure–temperature–time paths. Mineralogical Society of America Monograph, Washington, D.C.

Spear, F.S., Cheney, J.T., 1989. A petrogenetic grid for pelitic schists in the system SiO_2–Al_2O_3–FeO–MgO–K_2O–Na_2O–H_2O. Contributions to Mineralogy and Petrology 101, 149–164.

Spear, F., Daniel, C.G., 2001. Diffusion control of garnet growth, Harpswell Neck, Maine, USA. Journal of Metamorphic Geology 19, 179–195.

Spiess, R., Bell, T.H., 1996. Microstructural controls on sites of metamorphic reaction: a case study of the inter-relationship between deformation and metamorphism. European Journal of Mineralogy 8, 165–186.

Treagus, J.E., 1974. A structural cross-section of the Moine and Dalradian rocks of the Kinlochleven area, Scotland. Journal of the Geological Society of London 130, 525–544.

Tsuchiyama, A., Hanamoto, T., Nakashima, Y., Nakano, T., 2000. Quantitative evaluation of attenuation contrast of minerals in a medical X-ray CT scanner. Journal of Mineralogical and Petrological Sciences 95, 125–137.

Tsuchiyama, A., Nakamura, T., Nakano, T., Nakamura, N., 2002. Three-dimensional description of the Kobe meteorite by micro X-ray CT method: possibility of three-dimensional cyration of meteorite samples. Geochemical Journal in press.

Visser, P., Mancktelow, N.S., 1992. The rotation of garnet porphyroblasts around a single fold, Lukmanier Pass, Central Alps. Journal of Structural Geology 14, 1193–1202.

Wallis, S., 1992. Comment on "Do smoothly curved, spiral-shaped inclusion trails signify porphyroblast rotation?" Geology 20, 1054–1056.

Wallis, S.R., Behrmann, J.H., 1996. Crustal stacking and extension recorded by tectonic fabrics of the S.E. margin of the Tauern Window, Austria. Journal of Structural Geology 18, 1455–1470.

Yardley, B.W.D., 1977. An empirical study of diffusion in garnet. American Mineralogist 62, 793–800.

Zwart, H.J., 1962. On the determination of polymetamorphic mineral associations, and its application to the Bosost area (Central Pyrenees). Geologische Rundschau 52, 38–65.